we investigated the expression of GATA-2 and GATA-3 in WAT samples from several different models of murine obesity. These experiments demonstrated a severe reduction in the adipose expression of both GATA-2 and GATA-3 in four independent genetic models of obesity, including *ob/ob*, *db/db*, *tub/tub*, and *KKA^{Y} yellow*, in comparison to matched lean littermates (Fig. 5B). This reduced expression was specific to GATA, because AEBP-1 mRNA expression was not regulated in the obese animals and the level of the Pref-1 in adipose tissue was very low.

Our data demonstrate that GATA-2 and GATA-3 are preadipocyte genes, which act as molecular gatekeepers by controlling the transition from preadipocytes to adipocytes. Despite substantial changes in the architecture and the molecular complexity of adipose tissue, the biology of GATA factors at this site has been preserved from the fruit fly to the mouse. In higher organisms with balanced energy homeostasis, only a portion of the preadipocyte pool is used to become differentiated adipocytes. The remainder of the preadipocytes remains quiescent. Under the appropriate conditions, such as imbalance between energy intake and output, these cells differentiate into adipocytes and expand adiposity. If these control points fail, the result would be increased adiposity and, consequently, a higher tendency for obesity. The opposite will result in a loss of adiposity. Therefore, it is not surprising that the cellular machinery is equipped with molecules to control the rate and extent of transition between preadipocytes and adipocytes. The data presented here indicate that GATA factors are important regulators of this homeostatic mechanism and they may serve as targets for therapeutic intervention in diseases such as lipodystrophies and obesity.

References and Notes

1. B. M. Spiegelman and J. S. Flier, *Cell* **87**, 377 (1996).
2. S. Mandrup and M. D. Lane, *J. Biol. Chem.* **272**, 5367 (1997).
3. P. Tontonoz, E. Hu, B. M. Spiegelman, *Cell* **79**, 1147 (1994).
4. Z. Cao, R. M. Umek, S. L. McKnight, *Genes Dev.* **5**, 1538 (1991).
5. Z. Wu, Y. Xie, N. L. Bucher, S. R. Farmer, *Genes Dev.* **9**, 2350 (1995).
6. Z. Wu *et al.*, *Mol. Cell* **3**, 151 (1999).
7. T. Abel, A. M. Michelson, T. Maniatis, *Development* **119**, 623 (1993).
8. K. P. Rehorn, H. Thelen, A. M. Michelson, R. Reuter, *Development* **122**, 4023 (1996).
9. T. Evans and G. Felsenfeld, *Cell* **58**, 877 (1989).
10. S. F. Tsai *et al.*, *Nature* **339**, 446 (1989).
11. M. J. Weiss and S. H. Orkin, *Exp. Hematol.* **23**, 99 (1995).
12. Supplemental Web material is available at www.sciencemag.org/feature/data/1053426.shl.
13. Q. Tong and G. S. Hotamisligil, unpublished data.
14. W. S. Pear, G. P. Nolan, M. L. Scott, D. Baltimore, *Proc. Natl. Acad. Sci. U.S.A.* **90**, 8392 (1993).
15. C. M. Smas and H. S. Sul, *Cell* **73**, 725 (1993).
16. G. P. He, A. Mulse, A. W. Li, H. S. Ro, *Nature* **378**, 92 (1995).
17. Y. Zhu *et al.*, *Proc. Natl. Acad. Sci. U.S.A.* **92**, 7921 (1995).
18. H. Y. Yang and T. Evans, *Mol. Cell. Biol.* **12**, 4562 (1992).
19. A. P. Tsang *et al.*, *Cell* **90**, 109 (1997).
20. The recombinant GATA was expressed as a fusion protein with GST in the pGEX-2T plasmid (Pharmacia). Following induction expression with 0.3 mM isopropyl-β-D-thiogalactopyranoside for 2 hours, the fusion protein is affinity-purified with glutathione Sepharose (Sigma).
21. C.-N. Ting, M. C. Olson, K. P. Barton, J. M. Leiden, *Nature* **384**, 474 (1996).
22. H. Xu, J. K. Sethi, G. S. Hotamisligil, *J. Biol. Chem.* **274**, 26287 (1999).
23. G. S. Hotamisligil, N. S. Shargill, B. M. Spiegelman, *Science* **259**, 87 (1993).
24. The 0.6-kb PPARγ2 proximal promoter fragment (nucleotides −603 to +62) was cloned into the pXP2 plasmid (American Type Culture Collection, Manassas, VA) and transfected into NIH 3T3 cells with GATA-2 or GATA-3 expression plasmids by using the calcium phosphate method. *Renilla* luciferase reporter was used as an internal control for transfection efficiency. The deleted amino acids in ΔNzf (deletion of the amino zinc finger), ΔCzf (deletion of the carboxyl zinc finger), and ΔC+Nzf (deletion of both zinc fingers) are residues 281 through 313, 342 through 367, and 281 through 367, respectively, for GATA-2 and 257 through 287, 317 through 341, and 257 through 341, respectively, for GATA-3.
25. The electrophoretic mobility shift assays were performed in a 20-μl reaction volume. Two microliters of GST-GATA fusion protein was incubated with 0.5-μg poly[d(I-C)] and ^{32}P-labeled DNA probe (4×10^4 cpm) in the presence or absence of 1 μg of specific or nonspecific competitors, at room temperature for 20 min. The sequence of the specific competitor is 5′-GATCTCCGGCAACTGATAAGGATTCCCTG-3′ (underlined sequence indicates GATA recognition site), and the sequence of the nonspecific competitor is 5′-GATCGAACTGACCGCCCGCGGCCCGT-3′.
26. C. Dani *et al.*, *J. Cell. Sci.* **110**, 1279 (1997).

27. We thank S. H. Orkin for GATA-1, GATA-2, and GATA-3; D. B. Wilson for GATA-4; M. S. Parmacek for GATA-5 and GATA-6; H. S. Sul for Pref-1; H. S. Ro for AEBP-1 cDNAs; J. R. Reddy for PPARγ; and F. Saatcioglu for estrogen and thyroid receptor response element–driven reporter constructs. Q.T. is a recipient of the National Research Service Award (F32DK09940). The work is supported partially by NIH grants to J.M.L. (R37AI29673) and G.S.H. (DK56894) and by the Biomedical Scholar award from the Pew Foundation to G.S.H.

23 June 2000; accepted 21 August 2000

Proximity of Chromosomal Loci That Participate in Radiation-Induced Rearrangements in Human Cells

Marina N. Nikiforova,[1,2] James R. Stringer,[3] Ruthann Blough,[5] Mario Medvedovic,[4] James A. Fagin,[2] Yuri E. Nikiforov[1]*

Rearrangements involving the *RET* gene are common in radiation-associated papillary thyroid cancer (PTC). The *RET*/PTC1 type of rearrangement is an inversion of chromosome 10 mediated by illegitimate recombination between the *RET* and the *H4* genes, which are 30 megabases apart. Here we ask whether despite the great linear distance between them, *RET* and *H4* recombination might be promoted by their proximity in the nucleus. We used two-color fluorescence in situ hybridization and three-dimensional microscopy to map the positions of the *RET* and *H4* loci within interphase nuclei. At least one pair of *RET* and *H4* was juxtaposed in 35% of normal human thyroid cells and in 21% of peripheral blood lymphocytes, but only in 6% of normal mammary epithelial cells. Spatial contiguity of *RET* and *H4* may provide a structural basis for generation of *RET*/PTC1 rearrangement by allowing a single radiation track to produce a double-strand break in each gene at the same site in the nucleus.

Chromosomal rearrangements involving the *RET* gene are highly prevalent in radiation-induced thyroid tumors from children exposed to environmental radiation after the Chernobyl accident (*1–3*) and in thyroid cancers from patients with a history of medical external irradiation (*4*). They can also be detected 48 hours after exposing either human fetal thyroid explants or undifferentiated thyroid carcinoma cells to x-rays (*5*, *6*). Two common types of *RET* rearrangement in PTCs are intrachromosomal inversions that fuse the DNA sequence encoding the tyrosine kinase domain of *RET* with a portion of either the *H4* gene (*RET*/PTC1) or the *ELE1* gene (*RET*/PTC3) (*7*, *8*). In most *RET*/PTC3 tumors, the *ELE1-RET* fusion gene is formed by joining *ELE1* intron 5 to *RET* intron 11 by illegitimate recombination events, most of

[1]Department of Pathology and Laboratory Medicine, [2]Division of Endocrinology and Metabolism, [3]Department of Molecular Genetics, and [4]Center for Biostatistical Services, University of Cincinnati College of Medicine, Cincinnati, OH 45267, USA. [5]Cytogenetics Laboratory, Division of Human Genetics, Children's Hospital Medical Center, Cincinnati, OH 45229, USA.

*To whom correspondence should be addressed. E-mail: Yuri.Nikiforov@uc.edu

which conserve all of the DNA in both genes (*9*). Previous analysis of the *RET*/PTC3 breakpoint sites in 12 post-Chernobyl tumors showed that the tumors were all different with respect to the exact intronic sites at which *ELE1-RET* fusion occurred, suggesting that the breaks that mediated illegitimate recombination could occur anywhere within the two introns (*9*). It was, therefore, surprising that the two breakpoints associated with the formation of the *ELE1-RET* fusion in a given tumor tended to be located directly across from each other when the *ELE1* intron 5 was aligned with the inverse orientation of the *RET* intron 11 (*9*). This pattern of breakpoint positions suggested that these genes might be aligned and adjacent to each other in the nucleus at the time that double-strand breaks (dsb) were induced by radiation. To assess the spatial proximity of the *RET* locus to one of its recombination partners, we chose to study the *H4* locus, because *H4* is 30 Mb away from *RET* (whereas *RET* and *ELE1* are about 0.5 Mb apart), thus allowing accurate measurements of interphase distances by fluorescence in situ hybridization (FISH). In addition, a probe (D10S539) for a locus between *RET* and *H4* was available (*10*).

Normal thyroid cells were obtained from four unrelated adult individuals. The primary cultured cells were hybridized with *RET* and *H4* or *RET* and D10S539 probes (*11*). The three-dimensional (3D) microscopy showed that in 35% (93/263) of interphase nuclei of thyroid cells, at least one pair of *RET* and *H4* signals were juxtaposed (Fig. 1, A to D). To exclude the possibility that the high frequency of *RET* and *H4* juxtaposition was due to the presence of a *RET*/PTC1 rearrangement in a subpopulation of these presumably normal thyroid cells, 10 to 20 metaphase spreads per individual were analyzed on the same slides (Fig. 1E). The green (*RET*) and red (*H4*) signals were separated in all metaphases studied, and the orientation of *RET* and *H4* signals relative to the centromere was identical on both chromosome 10 homologs and corresponded to the expected positions of these genes along the linear map of chromosome 10. Additional confirmation of the absence of a *RET*/PTC1 rearrangement in these cells was obtained by reverse transcriptase polymerase chain reaction (RT-PCR) (*12*). The sensitivity of the reaction was sufficient to detect cells with a *RET*/PTC1 rearrangement mixed with cells that lack this rearrangement in a ratio of 1:1000. Thyroid cells from each donor were studied and showed no evidence of *RET*/PTC1 transcripts (*13*).

The prevalence of cells with at least one juxtaposed pair of *RET* and *H4* signals ranged from 29 to 40% in the four individuals (29, 30, 36, and 40%). This variation was not statistically significant ($P = 0.76$, Fisher's exact test). Of 93 nuclei that had at least one pair of juxtaposed *RET* and *H4* loci, five nuclei had two pairs of juxtaposed signals. The number of cells with both pairs of signals juxtaposed was not different from that expected by chance ($P = 0.11$) (*14*), indicating that juxtaposition of one pair of genes neither prevented nor stimulated juxtapositioning of the other pair.

By contrast with the data for *H4*, only 6% (14/256) of thyroid cells had *RET* juxtaposed to the D10S539 locus in three individuals (3, 5, and 7%, a nonsignificant interpersonal variation, $P = 0.53$). The difference between the frequency of association of *RET* with *H4* and *RET* with DS10S539 was highly significant ($P < 0.0001$).

In the second stage of analysis, the two-

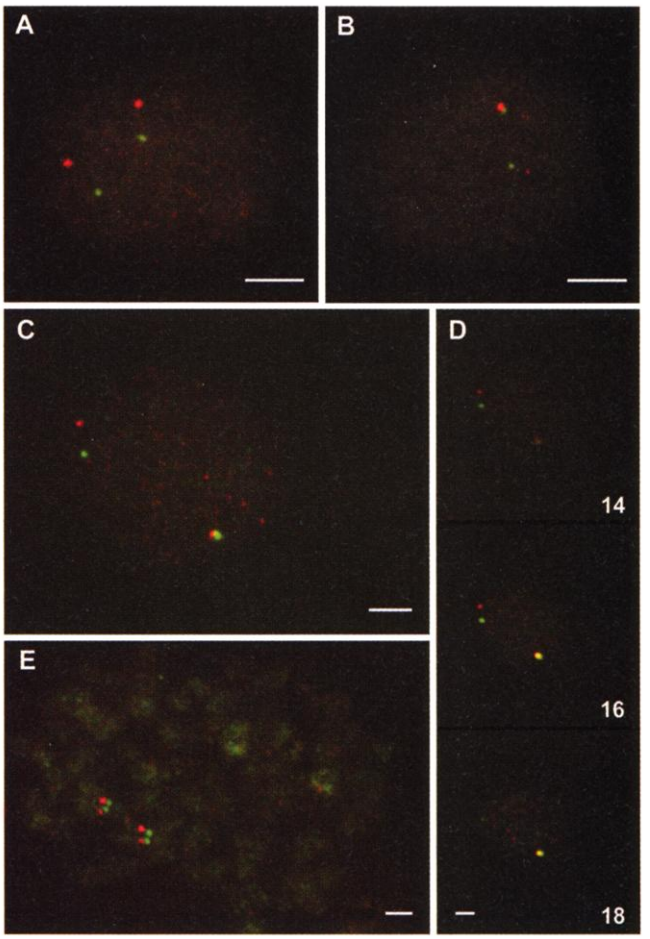

Fig. 1. Two-color FISH of normal thyroid cells with the *RET* probe (RMC10P013, green spots) and the *H4* probe (29F6, red spots). First, cells were viewed by 2D microscopy to identify cells where both pairs of RET and H4 signals were separated (**A**) and cells with at least one pair of adjacent *RET* and *H4* signals (**B** and **C**). Cell in the latter group were then visualized in 3D by viewing 30 optical sections of each nucleus. Signals were scored as juxtaposed if they were seen touching or overlapping each other in at least one optical section. To illustrate, the juxtaposed signals in (C) were seen in optical sections 16 to 18 (**D**). A metaphase spread was analyzed on the same slide showing separated *RET* and *H4* signals on both sister chromatids of both homologs of chromosome 10 (**E**). The RET signals on sister chromatids are closer together than the H4 signals are as expected because the RET gene is closer to the centromere. Scale bar, 3 μm.

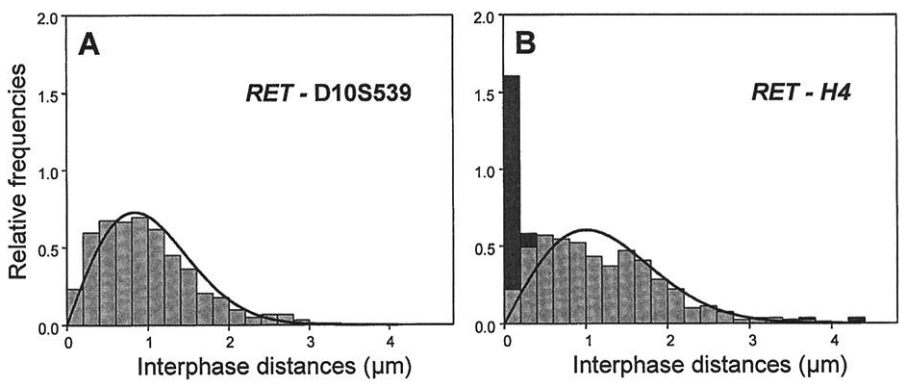

Fig. 2. Distribution of interphase distances between *RET* and D10S539 (**A**) and *RET* and *H4* (**B**) in thyroid cells as compared with the theoretical Rayleigh distribution (solid line). Dark bars indicate the measurements that were in excess of the number expected on the basis of the Rayleigh distribution (*19*).

dimensional (2D) *RET* to *H4* and *RET* to D10S539 distances were measured in interphase nuclei (*15*). The *RET* to D10S539 distances ranged from 0 to 3.32 μm and the *RET* to *H4* distances from 0 to 4.34 μm, which was consistent with the known positions of these three loci on chromosome 10; D10S539 is in between *RET* and *H4*. The distributions of these distances were then compared with a theoretical Rayleigh distribution, as calculated from a polymer model (*16*, *17*). Linear polymers can be considered as long, flexible molecular chains that fold in a random manner. Previous studies have shown that 2D interphase distances between chromosomal loci that are greater than 10 Mb apart do, in fact, conform to the Rayleigh distribution (*18*). The distribution of distances between *RET* and D10S539 conformed to the Rayleigh distribution, indicating that the spatial relation between these two loci was dominated by random influences (Fig. 2A). As can be seen in Fig. 2A, the Rayleigh distribution predicts that random factors will cause *RET* and another locus on the same chromosome to be close to each other in a small fraction of cells, hence the fact that *RET* juxtaposed to D10S539 in 6% of thyroid cells may have been due to chance, because there was no evidence of a specific association between these loci. By contrast, the distribution of *RET* and *H4* distances showed marked deviation from the Rayleigh model (Fig. 2B). This was primarily due to the signals that were either juxtaposed or closer than expected. Thus, out of 526 measurements, a statistically significant deviation was found predominantly in the 0- to <0.2-μm range (125 actual measurements compared with 13 expected by chance) and in the 0.2- to <0.4-μm range (43 compared with 36 expected) (*19*). The remainder of the distribution conformed to the Rayleigh curve, except for a slight excess in the number of cells in which the signals were at least 3.6 μm apart (four compared with one expected). These results provide further evidence that the *RET* and *H4* loci are nonrandomly associated in the nuclei of thyroid cells.

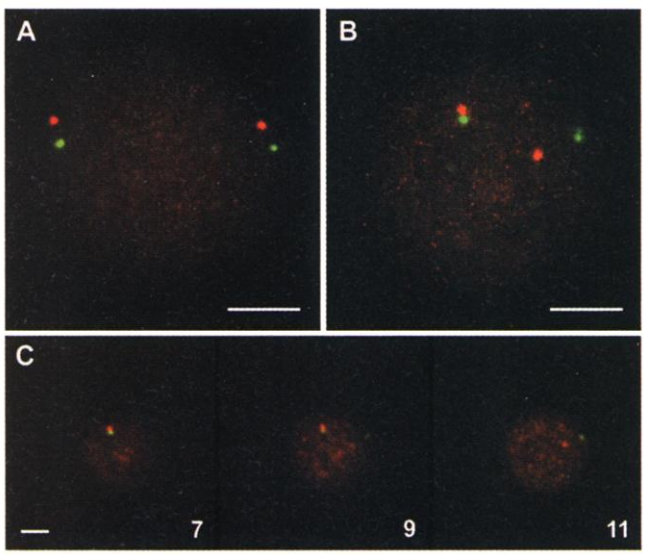

Fig. 3. Two-color FISH of PBLs with the *RET* probe (RMC10P013, green spots) and the *H4* probe (29F6, red spots). 2D image of nuclei showing two pairs of signals at a distance (**A**) and one pair of adjacent RET and H4 signals (**B**). The latter cell was scored as positive for juxtaposition because RET and H4 signals were seen touching each other in optical sections 7 to 9 (**C**). Scale bar, 3 μm.

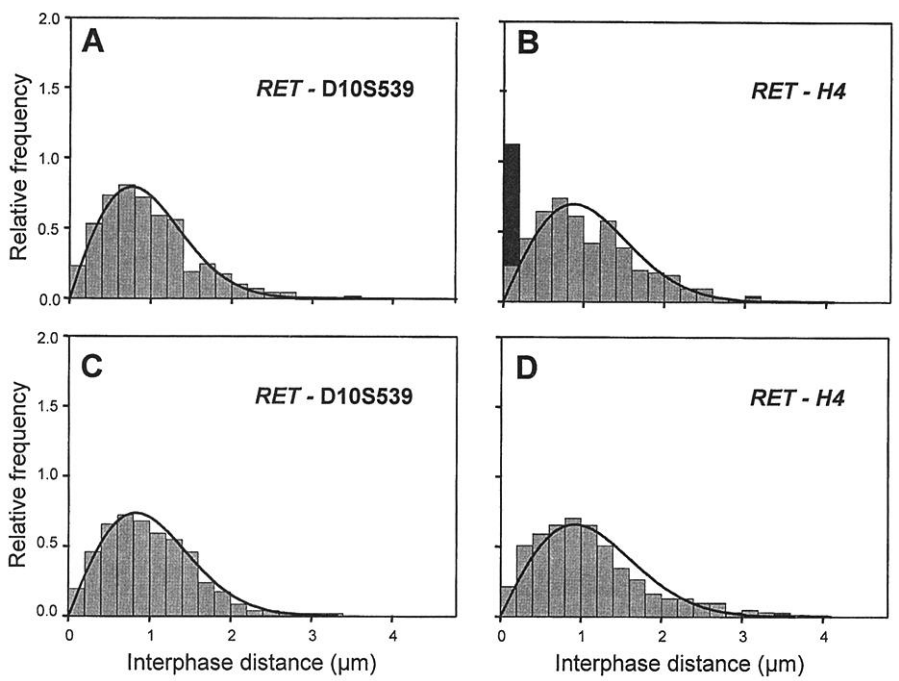

Fig. 4. Distribution of interphase distances between *RET* and D10S539 and *RET* and *H4* in PBLs (**A** and **B**) and NME cells (**C** and **D**) and the theoretical Rayleigh distribution (solid line). The dark bar indicates the measurements that were in excess of the number expected on the basis of the Rayleigh distribution (*19*).

The juxtapositioning of *RET* and *H4* was commonly observed in thyroid cells, raising the question of whether interphase proximity of these loci is a general feature of human cells. To address this question, we studied the interphase distances between *RET*, *H4*, and D10S539 in two additional cell types, peripheral blood lymphocytes (PBLs) and normal mammary epithelial (NME) cells (*20*). PBLs showed *RET-H4* juxtaposition in 21% (39/182) of cells (Fig. 3) and *RET*-D10S539 juxtaposition in 4% (8/180) of cells. In NME cells, *RET* and *H4* were juxtaposed in 6% (9/153) of cells and *RET* and D10S539 in 5% (6/114) of cells. The difference between the frequency of *RET*-H4 and *RET*-D10S539 juxtaposition was highly significant in PBLs ($P < 0.0001$), but not in NME cells. The frequency of *RET*-D10S539 juxtaposition was similar in all cell types studied.

Analysis of 2D interphase distances between *RET-H4* and *RET*-D10S539 showed that the *RET-H4* distances were not random in PBLs, whereas all other sets of measurements largely conformed to the Rayleigh distribution (Fig. 4). Hence, the association between *RET* and *H4* is not a universal feature of human cells, although it is definitely present in cells other than the thyroid.

Despite more than 50 years of study, the mechanism by which radiation produces chromosomal rearrangements remains unclear. Regarding *RET*/PTC1 rearrangements specifically, the problem can be reduced to understanding how the *RET* and *H4* genes, which share little sequence identity and are 30 Mb apart, become joined. The high frequency with which the *RET* and *H4* loci are juxtaposed offers an explanation by placing both potential recombination partners at the same place in the nucleus. Colocalization would serve to make these genes vulnerable to simultaneous incision by a single radiation track. The breaks produced will be very near

each other, creating the opportunity for ends to join cross-wise to produce a rearrangement. It is relevant to point out here that we recently found that in post-Chernobyl thyroid tumors with *RET*/PTC3 rearrangement, the breakpoints in the *RET* and *ELE1* genes tended to be located across from each other, which would be expected if they were a result of concerted dsb produced by a single radiation track in two adjacent chromosomal loci (*9*).

If *RET-H4* proximity facilitates formation of *RET*/PTC1 in irradiated thyroid cells, then gene proximity would be implicated in susceptibility to radiation-induced cancer. The *RET*/PTC1 chimeric gene has been shown to be able to cause thyroid cancer and mammary cancer in transgenic mice (*21*, *22*). Yet, *RET*/PTC1 rearrangements are not found in breast cancers in humans (*23*). In light of our findings, it is reasonable to postulate that *RET*/PTC1 rearrangements in human mammary cells are rare because the *RET* gene is not usually near its translocation partner in these cells.

Our data also show that a high frequency of *RET-H4* juxtaposition can occur in human cells that are not known to suffer oncogenic *RET*/PTC1 rearrangements, i.e., lymphocytes. Data from transgenic mice expressing *RET*/PTC1 suggest an explanation. Although they have the *RET*/PTC oncogene, these animals do not develop lymphomas, suggesting that lymphocytes may be resistant to *RET*/PTC-mediated transformation. Perhaps signaling through the *RET* tyrosine kinase is not sufficient for transformation of mouse lymphocytes. The same may be true in human lymphocytes.

The concept that two loci are able to participate in a radiation-induced chromosomal rearrangement because they are very close to each other in the nucleus is not new [reviewed in (*24*)]. However, little direct evidence of juxtapositioning of loci is available. The *BCR* and *ABL* genes, which are on different chromosomes, were reported to be located less than 0.3 μm apart in 2 to 8% of normal human lymphocytes (*25*). However, this frequency of proximity could be considered to be marginally higher than background taking into account that the data were collected with 2D analysis.

The frequency of *RET* and *H4* contiguity we report here is far and away the most striking example of spatial association between heterologous genes yet described. The high rate of these gene interactions in interphase nuclei would provide a structural basis for occurrence of *RET*/PTC rearrangements in human thyroid cells.

References and Notes

1. L. Fugazzola *et al.*, *Cancer Res.* **55**, 5617 (1995).
2. S. Klugbauer, E. Lengfelder, E. P. Demidchik, H. M. Rabes, *Oncogene* **11**, 2459 (1995).
3. Y. E. Nikiforov, J. M. Rowland, K. E. Bove, H. Monforte-Munoz, J. A. Fagin, *Cancer Res.* **57**, 1690 (1997).
4. A. Bounacer *et al.*, *Oncogene* **15**, 1263 (1997).
5. T. Mizuno, S. Kyoizumi, T. Suzuki, K. S. Iwamoto, T. Seyama, *Oncogene* **15**, 1455 (1997).
6. T. Ito *et al.*, *Cancer Res.* **53**, 2940 (1993).
7. M. Grieco *et al.*, *Cell* **60**, 557 (1990).
8. M. Santoro *et al.*, *Oncogene* **9**, 509 (1994).
9. Y. E. Nikiforov, A. Koshoffer, M. Nikiforova, J. Stringer, J. A. Fagin, *Oncogene* **18**, 6330 (1999).
10. G. H. Jossart *et al.*, *Cytogenet. Cell Genet.* **75**, 254 (1996).
11. Normal thyroid cells were obtained from freshly excised nonneoplastic portions of thyroid glands removed for benign nodules as previously described (*26*). Cells were plated directly on cover slips and kept in RPMI-1640 with 0.5% fetal bovine serum (FBS) without medium change for 2 to 3 days, resulting in ~90% of cells being in cell cycle stage G_0 or G_1 as detected by flow cytometric analysis. For FISH, cells were treated with 24 mM hypotonic sodium citrate buffer and fixed in three changes of 3:1 methanol:acetic acid. Probes used included P1 clones RMC10P013, corresponding to the *RET* gene; 29F6, corresponding to the *H4*/D10S170 gene; and RMC10P016, corresponding to the D10S539 locus. The order of these probes on 10q was reported by Jossart *et al.* (*10*). The *RET* probe was labeled with biotin-16-deoxyuridine triphosphate (dUTP); the *H4* and D10S539 probes were labeled with digoxigenin-11-dUTP (Boehringer-Mannheim). Two-color hybridization was performed as described elsewhere (*27*) and detected with fluorescein isothiocyanate (FITC) avidin and rhodamine-labeled antibody to digoxigenin (Oncor). Nuclei were counterstained with 4′,6′-diamidino-2-phenylindole (DAPI) in an antifade solution. Microscopy was performed with a Leica TCS 4D confocal laser scanning fluorescence microscope with digital image capture. A triple-band pass filter was used to view FITC, rhodamine, and DAPI fluorescence simultaneously. Nuclei were selected for analysis according to the following criteria: (i) adequate morphological preservation of nuclear shape and chromatin (as assessed by DAPI in antifade solution staining) and (ii) the presence of all four distinct hybridization signals. For each nucleus, 30 optical sections were obtained. The average increment between sections along the *z* axis was 0.2 μm. Images were photographed and stored in a digital format.
12. RNA was extracted from a portion of cells harvested from each donor and analyzed separately by RT-PCR with primers flanking the *H4-RET* fusion point in *RET*/PTC1 as previously described (*3*). The sensitivity of the reaction was tested by amplifying RNA extracted from a mixture of cells with *RET*/PTC1 with cells that lack the rearrangement. RNA integrity was monitored by amplification of *N-RAS* mRNA.
13. M. N. Nikiforova *et al.*, data not shown.
14. If 98 juxtaposed pairs are randomly distributed among 263 nuclei, the expected number of nuclei with two, one, and zero pairs of juxtaposed signals is 9, 80, and 174, respectively. Whether the observed numbers (5 cells with two, 88 cells with one, and 170 with zero juxtaposed signals) deviated significantly from this expected distribution was assessed by the exact conditional test (*28*).
15. 2D digital images were analyzed after enlargement to a magnification of up to 100, and in each nucleus the distances between fluorescent spots were measured in μm. The two *RET* and two *H4* or D10S539 signals were separated by four possible distances. However, in most cells, two pairs of heterologous signals were located in two separated areas of the nucleus with the distances between these heterologous pairs being several times shorter than another possible distance between heterologous signals (for example, Fig. 1, A to C, or Fig. 3, A and B). Thus, we assumed that the two shorter distances were between loci on the same chromosome.
16. G. Van den Engh, R. Sachs, B. J. Trask, *Science* **257**, 1410 (1992).
17. R. K. Sachs, G. van den Engh, B. Trask, H. Yokota, J. E. Hearst, *Proc. Natl. Acad. Sci. U.S.A.* **92**, 2710 (1995).
18. H. Yokota, G. van den Engh, J. E. Hearst, R. K. Sachs, B. J. Trask, *J. Cell Biol.* **130**, 1239 (1995).
19. Probability distribution function for Rayleigh distribution with the parameter Γ is given by (*17*)

$$f_R(x \mid \Gamma) = \frac{x e^{-x^2/2\Gamma}}{\Gamma}$$

Given a random sample $(x_1, \ldots, x_M)$ of observations from the Rayleigh distribution, the maximum likelihood estimate for the parameter Γ is

$$\hat{\Gamma} = \frac{\sum_{i=1}^{M} x_i^2}{2M}$$

The portion of observed distances deviating from the theoretical distribution was determined by iteratively reducing the number of observations from categories having too many measurements. The categories were created by dividing the range of observed distances into 0.2-μm intervals. The deviation of observed number of distances falling in the *i*th category, $i = 1, \ldots, c$ ($c = 20$ for *RET*-D10S539 and $c = 22$ for *RET-H4*) from the number expected on the basis of the Rayleigh distribution was quantified as

$$\chi_i = \frac{(x_i - e_i)^2}{e_i}$$

where x_i is the number of distances falling in the *i*th category and e_i is the number of distances expected to fall in this category under the Rayleigh distribution. e_i's are calculated by estimating the parameter of the Rayleigh distribution from the data and then integrating the Rayleigh probability density function over the corresponding interval. The algorithm that identifies the portion of observations from each interval that deviate from the theoretical distribution proceeded by repeating the following steps. Step 1: Calculate $\hat{\Gamma}$ on the basis of the current data $(x_1, \ldots, x_m)$ and then e_i's on the basis of $f_R(\cdot \mid \hat{\Gamma})$. Step 2: Find $\chi_{max} = \max(\chi_1, \ldots, \chi_c)$ and the corresponding category c_{max}. Step 3: Randomly simulate 100 samples of m observations $(x_1^j, \ldots, x_m^j)$, $j = 1, \ldots, 100$ from $f_R(\cdot \mid \hat{\Gamma})$. For each sample, calculate corresponding $\hat{\Gamma}_j$ and χ^j_{max}. Step 4: If there are at most five χ^j_{max}'s that are equal to or larger than χ_{max} (significant at $\alpha = 0.05$ level), one data point is removed from the category c_{max} and steps 1 to 4 are repeated for the remaining data. Otherwise, the process stops.
20. PBLs were obtained as nonstimulated lymphocytes from peripheral blood of two healthy adult individuals. Two preparations of NME cells were established from surgical specimens of benign breast tissue. PBLs were dropped on a slide, and NME cells were grown directly on cover slips. Cells were fixed and hybridized as described for thyroid cells.
21. S. Jhiang *et al.*, *Endocrinology* **137**, 375 (1996).
22. G. Portella *et al.*, *Oncogene* **13**, 2021 (1996).
23. M. Santoro *et al.*, *Br. J. Cancer* **68**, 460 (1993).
24. J. R. K. Savage, *Mutat. Res.* **366**, 81 (1996).
25. S. Kozubek *et al.*, *Blood* **12**, 4537 (1997).
26. P. L. Arscott *et al.*, *Endocrinology* **138**, 5019 (1997).
27. L. A. Cannizzaro and G. Shi, in *Basic Cell Culture Protocols*, J. W. Pollard and J. M. Walker, Eds. (Humana, Totowa, NJ, 1997), vol. 75, chap. 26.
28. B. S. Weir, *Genetic Data Analysis II* (Sinauer, Sunderland, MA, 1996).

29. We thank H.-U. G. Weier and J. W. Gray for providing the P1 clones 29F6, RM10P013, and RMC10P016 and S. Heffelfinger and M. Stampfer for providing NME cells. Supported by a Thyroid Research Advisory Council Award from Knoll Pharmaceuticals (Y.E.N.) and in part by grants PO1 ES 05652-10 (J.R.S.) and CA 72597 (J.A.F.) from NIH. Dedicated to the memory of Tatiana Yevgenievna Strazdovskaya.

21 April 2000; accepted 25 July 2000